SURFACE AND INTERFACE ANALYSIS
Surf. Interface Anal. **29**, 411–421 (2000)

REVIEW

Structure of highly dispersed metals and oxides: exploring the capabilities of high-resolution electron microscopy†

S. Bernal,[1] R. T. Baker,[1] A. Burrows,[2] J. J. Calvino,[1]* C. J. Kiely,[2] C. López-Cartes,[1] J. A. Pérez-Omil[1] and J. M. Rodríguez-Izquierdo[1]

[1] Departamento de Ciencia de los Materiales e Ingeniería Metalúrgica y Química Inorgánica, Facultad de Ciencias, Universidad de Cádiz, Apdo 40 Puerto Real, 11510-Cádiz, Spain

[2] Department of Materials Science and Engineering, University of Liverpool, Liverpool L69 3BX, UK

The potential applicability of high-resolution electron microscopy (HREM), in combination with image analysis and image simulation tools, to retrieve structural information from nanometre-sized particles present in oxide-supported metal and oxide catalysts is analysed. Specifically, the possibilities and limitations of this technique to determine features such as the size, morphology and chemical nature of the particles, their surface structure and their structural relationship with the support are considered through the discussion of several examples.

The interpretation of a series of HREM images of Pt and Rh catalysts supported on cerium oxides after treatments under different redox environments illustrates the case of highly dispersed metals. In addition, the results obtained in this study provide an approximate picture of the evolution of metal–support interaction effects in this family of catalysts, which is closely related to three-way catalysts (TWCs). The results of a nanostructural investigation of two catalyst systems, one consisting of MgO-supported neodymia clusters and the second of vanadium–magnesium oxide also supported on MgO, provide the examples for supported oxide catalysts. These find application in oxidation reactions. For the former, the growth of neodymia in the form of rounded patches in a parallel orientation relationship with the support has been observed. For the vanadia-containing catalysts, the formation of a weakly ordered MgV_2O_4 spinel surface phase on the MgO support crystallites, after exposure to typical reaction conditions in the oxidative dehydrogenation of propane, has been confirmed. The structural relationship at the spinel/MgO interface has also been established.

KEYWORDS: high-resolution electron microscopy; supported metal catalysts; supported oxide catalysts; highly dispersed phases; image analysis; image simulation; Rh/CeO_2; Pt/CeO_2; neodymia/MgO; VMgO catalysts

INTRODUCTION

A great variety of catalysts contain active phases in the form of nanometre-sized particles, of metal or oxide, dispersed over the surface of a second carrier or support material.[1] The details of the bulk and surface structure of these particles are among the key factors that control their performance. Likewise, the interactions that can be established between the supported phase and the support can further modulate the intrinsic catalytic properties of the supported phase. Thus, in the particular case of metal catalysts supported on some reducible oxides the occurrence of so-called metal–support interaction effects has been reported.[2] Different hypotheses have been proposed to explain the origin of these effects: structural or chemical modifications in the metal or metal//support interface (burial of metal atoms within the support,[3] coverage of the metal particle surfaces by support overlayers[4] or the formation of metal–support intermetallic phases[5,6]); electronic perturbations of the metal band structure;[7] and the simultaneous action of both structural and electronic contributions.[8,9]

Investigation of the structure of these materials seems, therefore, an unavoidable requirement to understanding their functionality. Given that the structural features of interest fall within the nanometric or subnanometric size domain, the techniques based on electron probes with a characteristic high spatial resolving power seem particularly well suited to face this task. In this respect, several monographs in the literature[10–12] demonstrate that high-resolution electron microscopy (HREM) is a suitable technique to investigate the nanostructural details of catalytic materials. The improvements in resolution achieved in the last decade have allowed electron micrographs to be

* Correspondence to: J. J. Calvino, Departamento de Ciencia de los Materiales e Ingeniería Metalúrgica y Química Inorgánica, Facultad de Ciencias, Universidad de Cádiz, Polígono Rio San Pedro, s/n. Apdo 40 Puerto Real, 11510 Cádiz, Spain.
E-mail: jose.calvino@uca.es

† Invited paper presented at Ecasia'99, 4–8 October 1999, Seville, Spain.

Contract/grant sponsor: DGICYT; Contract/grant number: PB95-1257.

Contract/grant sponsor: CICYT; Contract/grant number: MAT96-0931.

Contract/grant sponsor: MEC; Contract/grant number: HB1997-0236.

Received 15 July 1999
Revised 29 November 1999; Accepted 29 November 1999

recorded in which the structure of very different catalysts is imaged at the atomic scale. This very attractive possibility has made HREM a potential source of detailed nanostructural information closely related to macroscopic properties and to the inherent performance of particular catalysts.

Nevertheless, to take full advantage of the information contained in the experimental HREM images, the use of image simulation and image processing techniques is necessary. As stated in Ref. 13, supported catalysts can be considered, from the point of view of HREM, as materials containing finite, nanometre-sized interfaces. Image simulation proves to be necessary to understand the influence on the image contrasts of the structural parameters that are specific to this type of system:[13] the size of the supported particle, the position of the particle over the support surface and the thickness of the crystallite support. Moreover, the interpretation of the contrasts contained in HREM images of supported catalysts by comparison with simulated images allows access to qualitative and quantitative information that cannot be extracted from a direct inspection or a simple geometric analysis of the images. Furthermore, image simulations allow us to detect possible sources of misinterpretation and also give us a reasonable estimation of the safe limits for the application of HREM.

This paper does not intend to review the applications of HREM in catalysis, rather it is intended to review our own experience[13–19] in the analysis of HREM images of supported metals and oxides by using an approach based on the combined use of experimental HREM images, image processing and image simulation.

EXPERIMENTAL

The experimental HREM images presented in this paper were obtained on the following catalysts: 5% Rh/TiO_2, 2.5% Rh/CeO_2, 4% Pt/CeO_2, 0.5% $Rh/Ce_{0.8}Tb_{0.2}O_2$, 5% $Pt/Ce_{0.8}Tb_{0.2}O_2$, 3% Nd_2O_3/MgO and VMgO catalysts with 14wt.% V content. They were recorded using a JEOL-2000EX electron microscope operating at 200 kV. The structural resolution of this instrument is 0.21 nm. Further details about the preparation of the samples and activation procedures can be found in Refs 14–16 and 19–21.

Simulated images were calculated using EMS software[22] and the structural models used as input for the simulations were built with the RHODIUS program developed at the University of Cadiz.[23] Both programs were run on an INDY 4400SC Silicon Graphics workstation. Image processing tasks were accomplished using the SEMPER 6+ package by Synoptics Ltd., on images digitized with a COHU-4910 CCD camera. The diffractograms or digital diffraction patterns (DDPs) included in this work correspond to the power spectrum of the Fourier transform of the bidimensional intensity distribution in the digitized images.

RESULTS AND DISCUSSION

The interpretation of an HREM image of a material made of particles dispersed over the surface of a support implies the search for qualitative/quantitative answers to the following questions, among others: what is the chemical composition of the small particles?; what are their sizes?; what are their shapes?; can anything be said about the surface structure? The same questions could be posed with respect to the support crystallites. Furthermore, details about the structure of the system as a whole are also of interest, as are those related to the particle//support interface. Although in the following text these topics are addressed in distinct monographic sections, it is important to note that in general it is not possible to separate them when interpreting a particular experimental image. In fact, to simulate a particular HREM image, a precise model of the system in which all the features mentioned above are fixed simultaneously has to be used.

Size of the supported particles

Figure 1(a) contains an HREM image showing a region, several tens of nanometres wide, of a 4% Pt/CeO_2 catalyst after reduction in hydrogen at 623 K. A portion of a CeO_2 support crystallite can be observed in which fringes corresponding to the (111) planes of the fluorite structure, at 0.312 nm, are resolved. In addition, smaller crystals, of a few nanometres dimension, sitting on the surface of the ceria crystal, are also readily recognized. These correspond to metallic Pt particles. Note that these Pt particles can be observed both along the boundary of the support, indicated by black arrows, and also in the inner region of the image (indicated by white arrows), superimposed over the contrasts corresponding to the (111) ceria fringes. In the former case, particles and therefore the metal//support interface are imaged in the so-called profile view projection, whereas in the latter the image corresponds to a plan or top view projection[24] of the metal//support system. The particles that are imaged in top view can be located either by the observation of local lower brightness regions or by the observation of large spacing, high contrast and wide Moiré-type fringes that arise from double diffraction effects.[25] In any case a simple visual inspection of the experimental image allows the detection of the presence and location of the supported phase in a particular area of a catalyst particle.

This possibility of visualizing the individual particles present in the system allows a direct estimation of the particle size. Given that HREM is a projection technique, such an estimation would certainly correspond to the projected size. Although in the case of non-spherical particles different parameters could be used for the estimation of particle diameter,[26] once a precise protocol is chosen for such a measurement this can be applied to every particle detected in an image. If several tens of experimental images are analysed, the diameter of a few hundred supported particles can be measured. This opens the interesting possibility of establishing a distribution of particle sizes that is, very likely, one of the great advantages of HREM in the determination of this particular structural parameter. From these size distributions, parameters relevant to the catalytic performance, such as the mean particle diameter or the fraction of exposed atoms (dispersion), can be computed by using appropriate procedures.[27,28]

As an example, Fig 1(b) shows the histogram obtained from the analysis of the micrographs recorded for the 4% Pt/CeO_2 catalyst mentioned above. From this distribution an average particle diameter of $\sim$2.4 nm and a dispersion

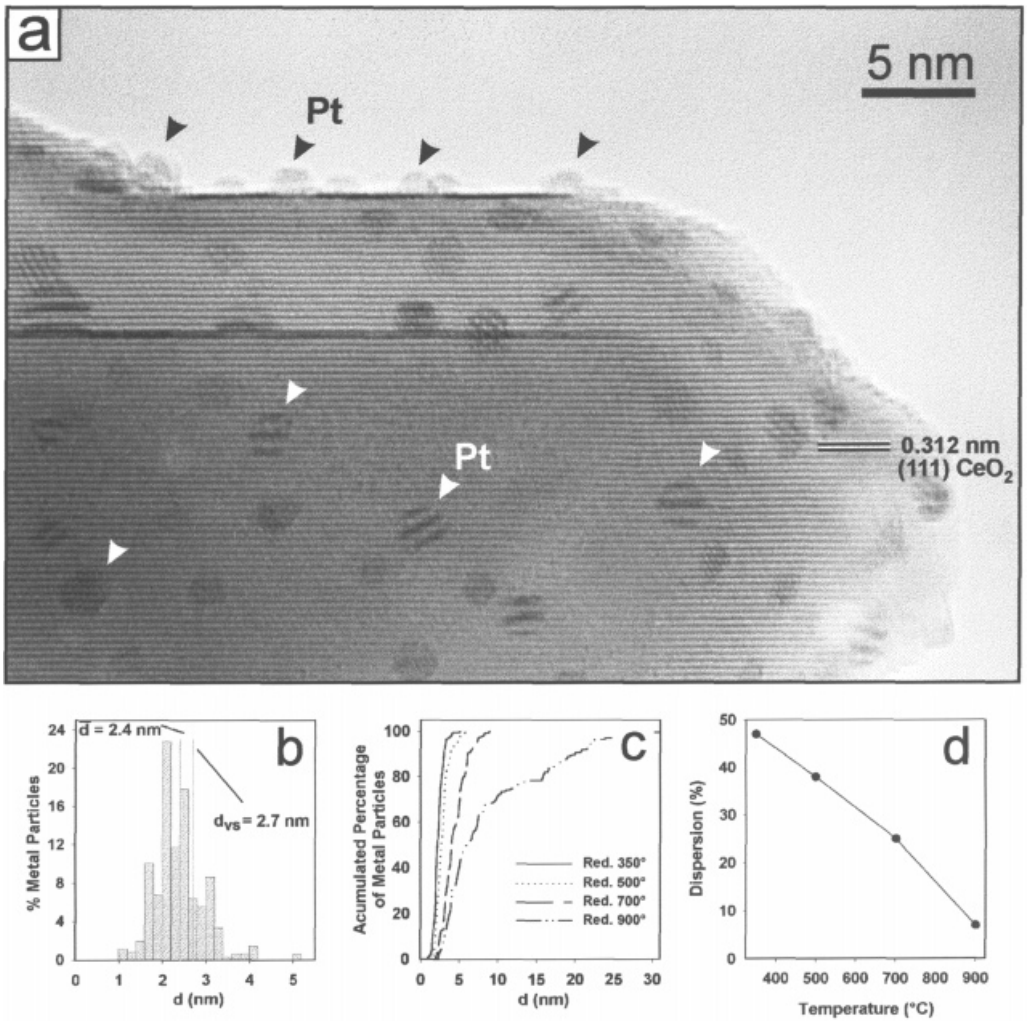

Figure 1. (a) The HREM image corresponding to the 4% Pt/CeO_2 catalyst reduced at 623 K. (b) Histogram of the particle size distribution of the same catalyst. (c) Integrated size distribution curves as a function of the reduction temperature. (d) Evolution of the dispersion of the supported phase with reduction temperature.

of 47% could be estimated.[17] Figure 1(c) shows the evolution of the integrated size distribution curves for the same catalyst, as a function of the reduction temperature within the range 623–1173 K. It seems clear that sintering of the metal particles is not very significant after reduction at 773 K but becomes dramatic after reduction at 1173 K. The dispersion of the metal phase [Fig. 1(d)] drops monotonically in the range 623–973 K, and then very steeply after reduction at 1173 K. Such data allow evaluation, in quantitative terms, of the ability of ceria to stabilize the metal dispersion, one of the roles commonly attributed in the literature to this oxide as a component of three-way catalysts (TWCs).[29]

To perform the estimation of particle size from HREM images no detailed contrast interpretation is required, only direct geometric measurements that can be performed simply with a ruler. Nevertheless, image simulation is required to establish the limits and degree of confidence of this estimation. In fact, calculations are required to determine both the size of the smallest particle that can be detected[13,30,31] and the deviation of the sizes estimated from the images from the real projected sizes of the particles.[13,32] Although these questions are microscope and sample dependent, in the case of supported metals, according to calculations included in these references, particles of 0.8–1.0 nm are still detectable. Furthermore, the technique is also shown to be reliable for samples with dispersions up to 80%. In Ref. 15 and 27 good agreement is found between dispersions obtained from HREM images and those determined from volumetric adsorption essays.

For samples with very high dispersions, the use of alternative techniques, such as extended x-ray absorption fine structure (EXAFS), is required. Actually the combined use of HREM and EXAFS would allow one to cover the whole spectrum of particle size in normal catalytic samples. To rule out the presence of extremely large particles, e.g. in samples presenting bimodal distributions, XRD or SEM–energy-dispersive spectroscopy (EDS) data can be helpful.[17] Analysis by SEM–EDS is especially important in cases where a significant fraction of metal particles involved in the upper end of the distribution is below the x-ray diffraction (XRD) detection limit.

Morphology of the supported particles

Figure 2 contains different examples relating to the analysis of the shape of nanoparticles using HREM. Images in the left column show experimental images recorded on different metal//support systems. Note the presence of well-faceted metal particles. The analysis of spacing

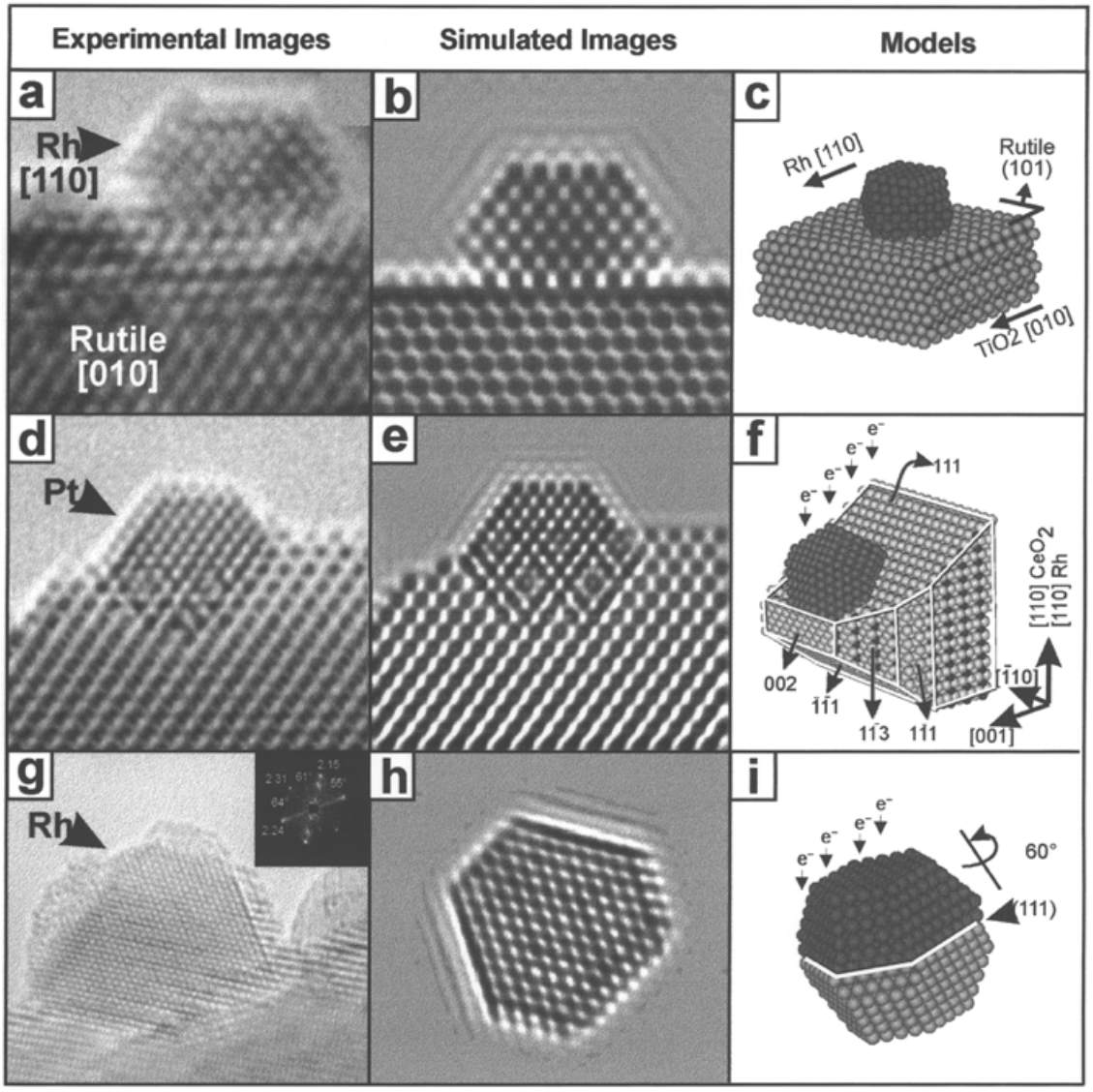

Figure 2. Experimental images corresponding to Rh/TiO_2 (a), 4% Pt/CeO_2 (d) and 2.5% Rh/CeO_2 (g) catalysts. (b, e, h) simulated images (c, f, i). Models used to obtain the simulations.

and angles between lattice fringes allows identification of the crystallographic planes exposed at the surface and the number of planes of each type involved in the projection. From this information a three-dimensional particle shape can be guessed and modelled. From these models, calculated images like those shown in the central column of Fig. 2 can be obtained. A good match between the experimental and simulated images is observed. Both the outline of the metal particles and the contrasts observed inside the particles are well reproduced in the calculations. In the three cases shown, the metal particle shapes are based on cuboctahedra (right column in Fig. 2). Thus, in the case of the image of the Rh/TiO_2 catalyst, the rhodium particle adopts the shape of a cuboctahedron with square {100} facets and triangular {111} facets.[15] The cuboctahedron is truncated on one of the (100) facets that is in contact with the (101) surface of a rutile support crystallite.

The second image [Fig. 2(d)] can be interpreted in terms of a (111)-truncated cuboctahedron of Pt with hexagonal-{111} and square {100} facets.[13] The particle is sitting on a (111) surface of a ceria crystal whose shape has also been defined in the calculation. The electron beam impinges on the sample along a direction a few degrees off [110], in such a way that the particle is being imaged simultaneously in profile and top view projections.

The third image was recorded on a 2.5% Rh/CeO_2 catalyst after reduction at a high temperature of 1173 K. As already seen in the previous section for the 4% Pt/CeO_2 sample, treatment under these conditions lead to severe sintering of the Rh particles.[27] The formation of twins or multiple twins is the usual consequence of sintering. Thus, the image of the rhodium particle in Fig. 2(g) can be explained in this case as being due to a Rh bicrystal comprising two cuboctahedral subunits contacting along one of their (111) planes. The upper cuboctahedron is rotated 60° about the (111) contact plane. The twinned particle in Fig. 2(i) is imaged in top view, down the [123] zone axis of the lower Rh subunit. Fringes corresponding to the (111) planes of the upper unit are superimposed in the image with the (111) fringes of the lower one, resulting in a cross-fringe pattern with 55°, 61° and 64° angles (shown in the DDP inset in the figure) that is nicely reproduced in the calculation. It is important to note that such a pattern cannot be interpreted as being due to any projection of the fcc structure of metallic rhodium. Taking into consideration the severe reduction conditions under

which the catalyst was treated, the formation of a possible Rh–Ce alloy could have been erroneously suggested as being responsible for this anomalous contrast pattern. Image simulation clearly indicates that this would have been a mistake and gives us a clear indication of the need to rely on calculations to interpret the contrasts observed in HREM images of these materials. Further references dealing with the study of twinned metal particles can be found in the literature: Ref. 33 and references therein, as well as Refs 34 and 35 related to the study of metals on amorphous supports.

Concerning the possibility of detecting deviations from ideal shapes, due for example to the presence of vacancies or steps on the metal surface, it is important to note that HREM images will be mainly sensitive to changes in those features of the morphology that, in projection, fall along the profile of the particle.[13] Likewise, the irregular growth of a particular set of planes will be detected readily for those planes included in the zone axis defined by the incident electron beam direction. Changes affecting the contrast inside the particle, i.e. imaged in plan view, will be in principle hardly detectable and very difficult to separate reliably from other image artefacts. Some authors have proposed[36] that from a precise determination, using image processing techniques, of the position of the contrast maxima observed in the HREM image of small particles with atomic resolution, the 'roughness' of metal particle surfaces can be estimated. In our opinion exhaustive image calculations performed on nanometre-shaped models and consideration of the influence of experimental parameters such as small crystal tilts would be necessary to deconvolute the contribution of artefacts to the image contrast.

Certainly, as already stated, HREM is a projection technique. However, it is also important to realize that an HREM image allows the observation of a large number of particles in different orientations. Hence, unless the sample is very inhomogeneous with respect to particle shape, which in fact is quite unusual, HREM allows one to extract a close approximation to a representative particle shape. Additional examples discussed in the following sections will enhance the discussion of this point.

Chemical nature of the supported particles

Figure 3 (left column) shows experimental images recorded on CeO_2-supported catalysts after being submitted to different thermochemical treatments. Figure 3(a) was recorded from a 2.5%Rh/CeO_2 catalyst reduced in pure hydrogen at 773 K and reoxidized in pure oxygen also at 773 K.[37] A rounded particle on the surface of a ceria crystallite is observed. A 0.374 nm spacing between the lattice fringes, characteristic of the (012) planes of the hexagonal-Rh_2O_3 phase, can be estimated. The image calculated for a structural model consisting of a spherical-shaped Rh_2O_3 particle down a zone axis a few degrees off the [010] direction [Fig. 3(b)] reproduces the (012) lattice fringes and, in general, matches quite well the contrast observed in the experimental image. This result confirms that the aforementioned treatment induces the transformation of the metallic particles formed after reduction at 773 K into the sesquioxide, in good agreement with Temperature Programmed Oxidation (TPO) data obtained for the same catalyst.[37]

Figure 3(c) corresponds to a 4% Pt/CeO_2 catalyst treated under reducing conditions in pure hydrogen at high temperature (1173 K). In this case a faceted supported particle ~6 nm in size showing a contrast pattern consisting of intensity maxima with hexagonal symmetry is observed. This contrast pattern cannot be assigned to any of the orientations of metallic Pt but, instead, to the [001] zone axis of a hexagonal $CePt_5$ intermetallic phase. Simulations obtained for this phase in the cited orientation [Fig. 3(d)] reproduce perfectly well the contrast pattern observed in the experimental recording.

Images obtained after the same treatment for a Pt catalyst supported on a mixed cerium–terbium oxide support indicate also an incorporation of the lanthanide elements present in the support into the structure of the metallic particles.[38] Thus, experimental images such as that shown in Fig. 3(e) can be explained fully with simulations based on models containing $LnPt_5$ (Ln : Ce, Tb) particles [Fig. 3(f)]. This intermetallic phase is isostructural with the binary $CePt_5$ phase. However, even with a detailed analysis of the contrasts observed in these particles it is still not possible to reach reliable conclusions about the content of the intermetallic in each of the lanthanide elements present in the support. Complementary measurements using nanoanalytical techniques (electron energy-loss spectroscopy, EELS) have been necessary to clarify this point.[38] The EELS data clearly indicate the preferential incorporation of Ce into the intermetallic phase.

To reproduce in the calculation the outline of the intermetallic particle observed in the experimental image shown in Fig. 3(e), a beryl-type morphology[39] was assumed. This morphology accounts for the preferential growth of the particles along the *c*-axis. The [001] projection of the $CePt_5$ intermetallic particle detected in the image of the Pt/CeO_2 catalyst [Fig. 3(c)] is also consistent with this morphology.

Figure 4 addresses phase recognition in a supported oxide system. The experimental plan view image was obtained on a 14 wt.% V/VMgO catalyst after exposure to pure propane at 773 K for 4 h.[19] Small patches of an ordered structure, enlarged in Fig. 4(b), can be distinguished. The DDPs of these patches [Fig. 4(c)] indicate the presence of periodicities of 0.495 and 0.469 nm intersecting at an angle of ~68°. These periodicities and interplanar angles are not consistent with any of the vanadium oxides V_2O_3, V_2O_4 or V_2O_5. These features can be explained if the formation of a MgV_2O_4 spinel is assumed. To confirm this proposal a model of a surface spinel phase supported on MgO with a parallel orientation relationship was built [Fig. 4(d)]. The images simulated for this model [Fig. 4(e)] reproduce quite well the contrast of the experimental images. Likewise, the DDPs obtained from these calculations [Fig. 4(f)] contain the fringe pattern features mentioned previously. This result confirms that during treatment in propane V^{5+} reduces to V^{3+} and is incorporated into the framework of a mixed phase in company with Mg^{2+} ions coming from the support. It is also worth noting that the patches grow with a well-defined crystallographic orientation relationship that allows the formation of a very smooth interface, with only a 0.23% mismatch. In fact, the oxygen sublattice retains its structure across the interface plane.

This last example illustrates the possibilities of HREM in the analysis of structures that show a preferential two-dimensional growth, in this case in the form of oxide patches imaged in plan view. The HREM images obtained

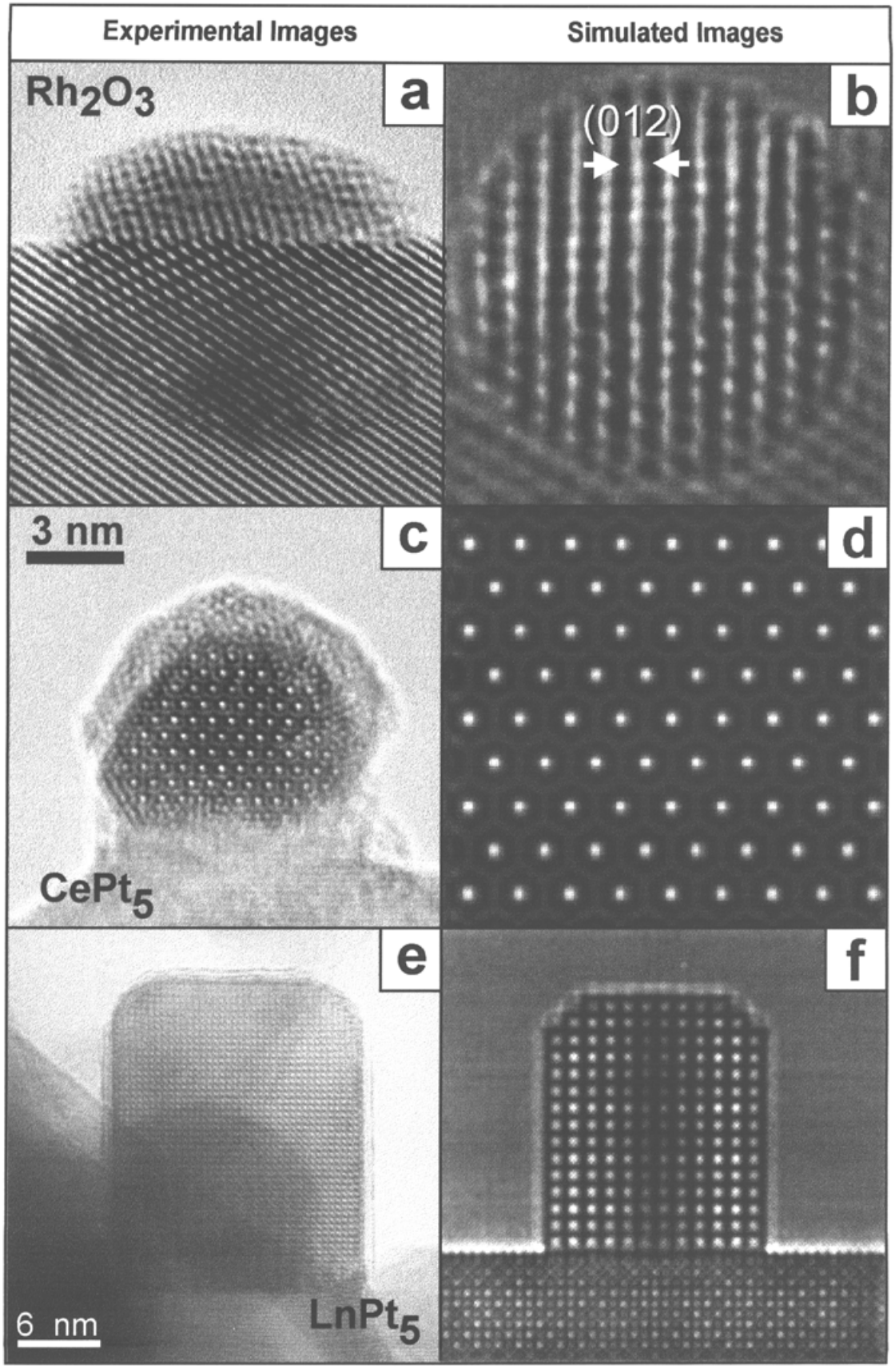

Figure 3. (a) The HREM image corresponding to the 2.5% Rh/CeO_2 catalyst reduced at 773 K and oxidized further at 773 K. (b) Simulated image obtained from a spherical particle of hexagonal Rh_2O_3. (c) Experimental image of the 4% Pt/CeO_2 system reduced at 1173 K. (d) Calculated image of the $CePt_5$ phase along the [001] direction. (e) Image corresponding to the 5% $Pt/Ce_{0.8}Tb_{0.2}O_2$ catalyst reduced in pure hydrogen at 1173 K. (f) Simulated image from a model consisting of an $LnPt_5$ alloy particle with beryl-type morphology supported on the mixed oxide.

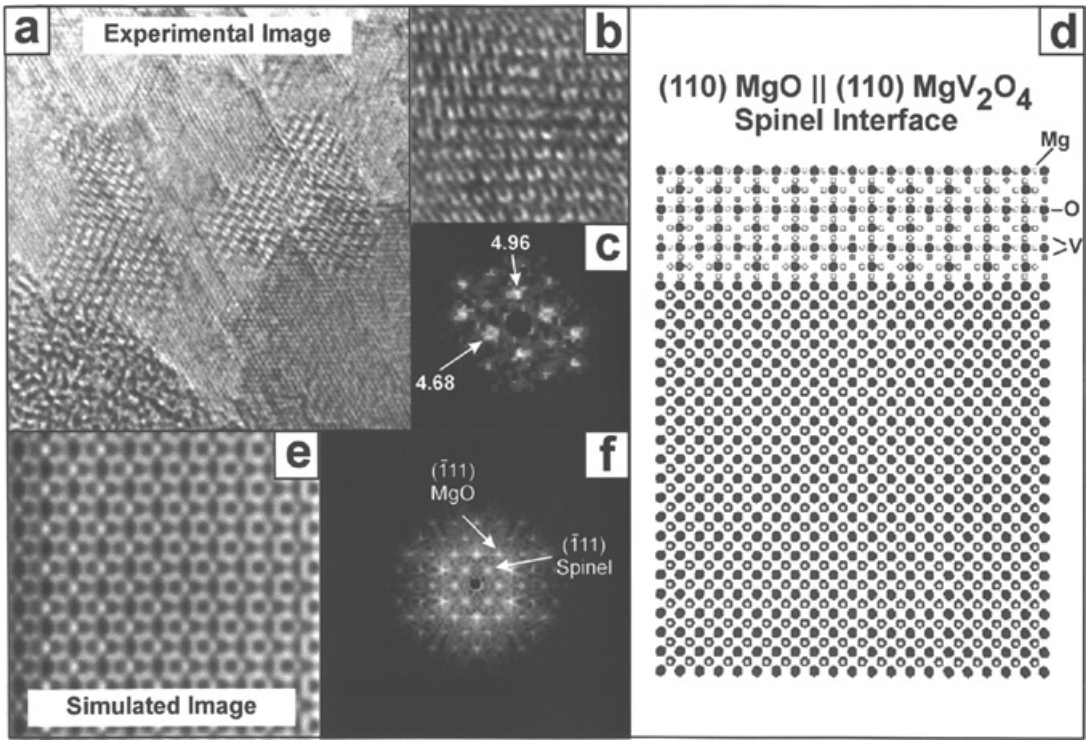

Figure 4. (a) Experimental image of a (14% V) VMgO catalyst after treatment in pure propane for 4 h. (b) Detail of the experimental image. (c) The DDP obtained from the experimental image. (d) Model used to run the simulation. (e) Simulated image. (f) The DDP from the simulated image.

in the same catalyst under profile projection indicate that these patches could be ~1–1.5 nm thick.[19]

Surface and interface details

Analysis of the image in Fig. 4(a) revealed that the supported MgV_2O_4 phase grew under a precise orientation relationship over the surface of the MgO support crystals. In supported metal systems the same effect is usually observed,[13–17,34,35,40] which reveals quite clearly the influence of the support surface structure on the growth of the small particles. High-resolution electron microscopy is very well suited to determine these correlations, both profile and plan view images being useful to characterize the structural features of metal//support interfaces.[14]

Figure 5 (left column) shows two experimental images recorded on ceria-based catalysts after reduction at low temperature. In the image recorded on the 0.5% $Rh/Ce_{0.8}Tb_{0.2}O_2$ catalyst [Fig. 5(a)], a parallel alignment between the (111) planes of the mixed oxide and the (111) planes of Rh is observed. The image indicates also that the metal particle has grown with one of its (111) planes over a (111) plane of the ceria crystal. According to the model shown in Fig. 5(c), this alignment can be explained by assuming an epitaxial growth of the metal particle over the support, which can be defined by the following crystallographic relationships:

$$(1-11)\ \mathrm{Rh}\|(1-11)\mathrm{Ce_{0.8}Tb_{0.2}O_2}\ \text{and}$$
$$[110]\ \mathrm{Rh}\|[110]\mathrm{Ce_{0.8}Tb_{0.2}O_2}$$

In Ref. 14 this orientation relationship is regarded as a parallel epitaxy. Figure 5(b) shows a calculation based on this model, matching the features of the experimental image.

The growth of Rh and Pt particles on ceria can alternatively occur under a twin epitaxy.[14,17] In this case [Fig. 5(d)] the (111) planes of the metal and the support are related by a (111)-mirror plane operation, as depicted by the twisted lines marked on the image. The equations that define the orientation relationship in this case are:

$$(1-11)\ \mathrm{Pt}\|(1-11)\mathrm{CeO_2}\ \text{and}\ [110]\ \mathrm{Pt}\|[011]\mathrm{CeO_2}$$

The parallel and twin epitaxies are related to each other by a 60° rotation about the (111) axis perpendicular to the surface plane. Given that the metal and support planes that are in contact at the interface both have, ideally, sixfold symmetry,[14] it turns out that the structure of the interface is exactly the same for both orientation relationships. This could explain why both topotaxies occur experimentally.

Moving to the field of supported oxides, Fig. 6 shows an experimental HREM image representative of a 3% Nd_2O_3/MgO catalyst as prepared. The image is characterized by a featureless, low-contrast background with some outstanding white dots in an ordered arrangement (region indicated by the arrow). Of the different structural models considered to reproduce these contrast features, the one showing the best match with the experimental image corresponds to a rounded, unstrained, monolayer raft of cubic Nd_2O_3 in [001] orientation grown under parallel orientation over a (001) surface of MgO:

$$\mathrm{Nd_2O_3}(001)\|\mathrm{MgO}(001)\ \text{and}\ \mathrm{Nd_2O_3}[100]\|\mathrm{MgO}[100]$$

Figures 6(d) and 6(e) show, respectively, a plan and an edge-on view of this model. A close match is observed between the image calculated for this model [Fig. 6(b)]

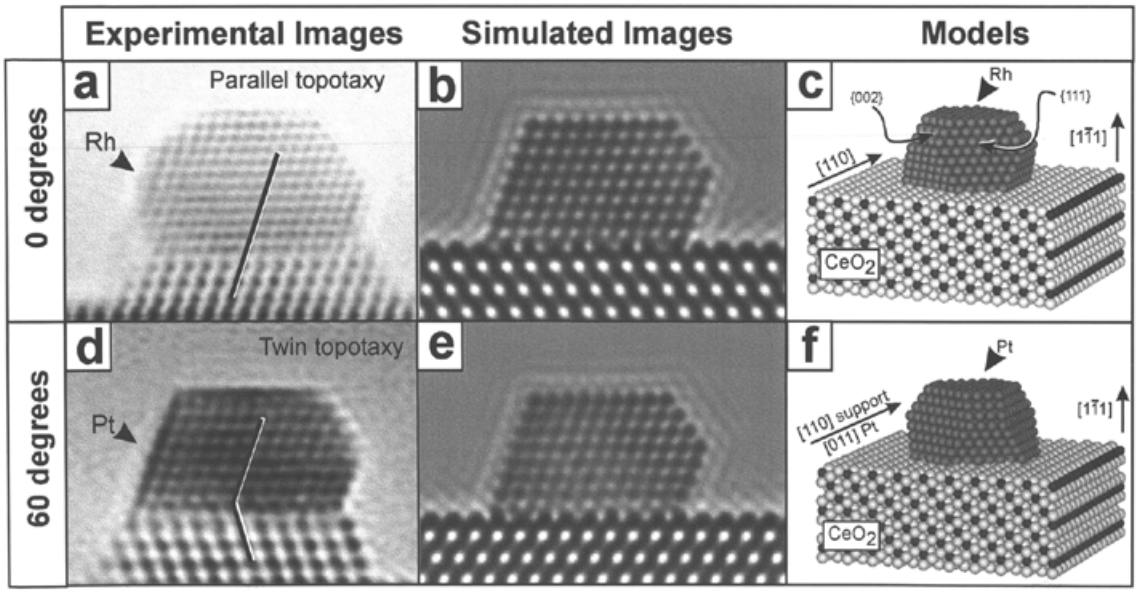

Figure 5. Experimental images from 0.5% $Rh/Ce_{0.8}Tb_{0.2}O_2$ (a) and 4%Pt/CeO_2 (d). (b, e) Calculated images for Rh- and Pt-supported particles. (c, f) Supercell models used to run the calculations.

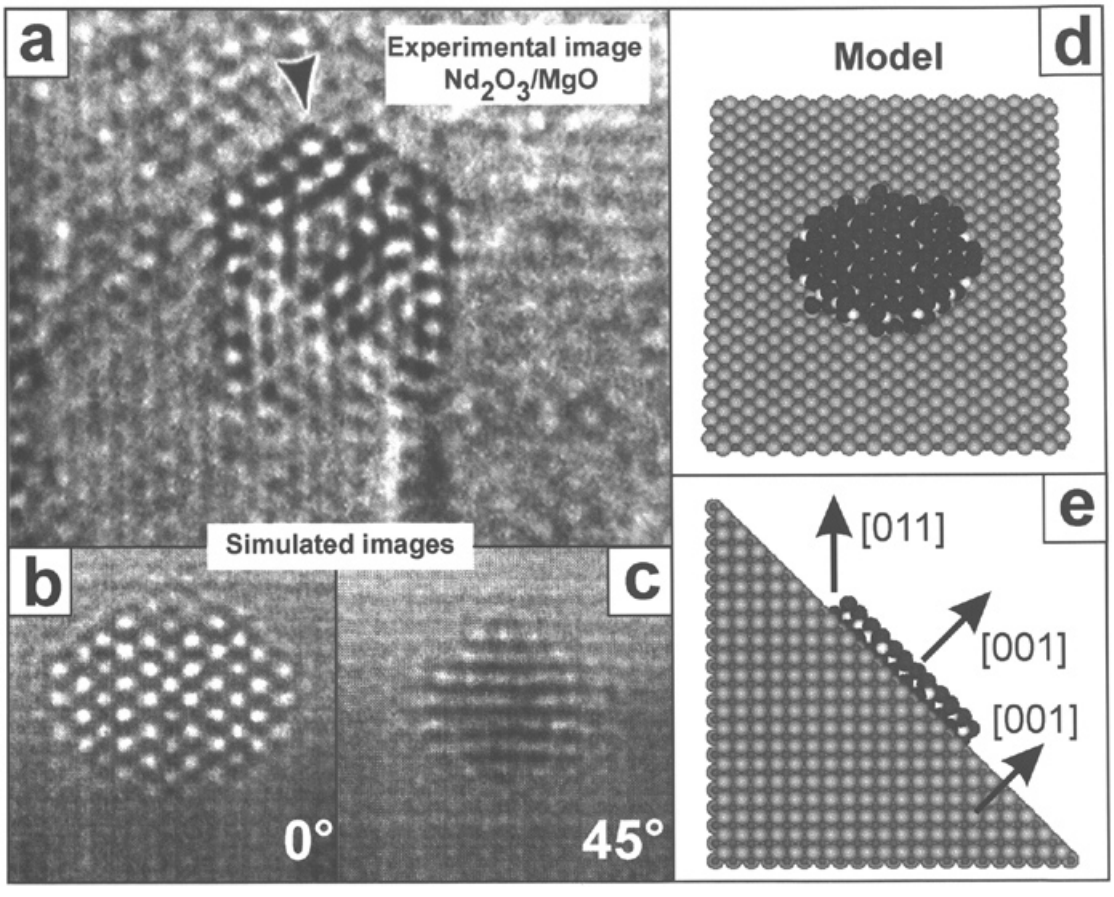

Figure 6. (a) The HREM image of a 3% Nd_2O_3/MgO catalyst. (b, c) Simulated images. (d) Plan view and (e) profile of the model built for the calculation.

and the experimental image. This model involves an incoherent interface in which there is near coincidence of every third Nd_2O_3 (400) plane with every fourth MgO (200) plane. The mismatch in this 3 : 4 arrangement would be only 1.6%.

A rotation of 45° of the neodymia cluster about the coincident [001] direction would lead to a coherent interface with a 7.2% mismatch. However, the simulated image for this second interface model [Fig. 6(c)] is far from the experimental recording. Note how the intense white dots have disappeared from the image after the rotation. This result provides an example of how sensitive the HREM images of supported phases are to changes in orientation relationships. It is also worth emphasizing that

in this particular case we have been dealing with a very challenging problem: the structure of interfaces involving nanosized two-dimensional crystals.

Additional features of these nanosized interfaces could be investigated using a strategy based on a match between experimental and simulated images, such as the distance between the planes contacting at the interface or the chemical nature of these planes.[13] In this case detailed interpretation of image contrasts is necessary. Hence, detailed calculations considering the influence of a large number of parameters are required for this purpose if reliable conclusions are to be drawn. Among these parameters, the thickness of the support crystallite and small crystal tilts play a major role in the distribution of contrasts in the image.[13,41] The polycrystalline nature of catalytic powders means that these parameters are completely unknown when reaching the interpretation step, and a large number of trials to fix them therefore becomes necessary.

Occasionally, new interfaces are developed in this type of material as a consequence of activation treatments or operating conditions. This is the case, for example, of Rh and Pt catalysts supported on CeO_2 or Ce–Tb mixed oxides. When these catalysts are treated in hydrogen at high temperature (above 973 K), thin layers of support migrate on top of the surface of the small metal particles. This decoration effect means that extension of the metal//support interface increases at the expense of covering a fraction of the metal particle surfaces that were clean, and therefore available to adsorbates or reactants, in the catalysts reduced at low temperatures. Figure 7(a) shows an experimental image of a 2.5% Rh/CeO_2 catalyst reduced in hydrogen at 1173 K for 1 h. It is apparent that the metal particle is surrounded, at the bottom part, by a ceria shell and also the presence of two layers of decoration covering partially the surfaces that are imaged in profile. Figure 7(b) shows an enlargement of this coverage where its crystalline nature can be appreciated clearly. Analysis of the lattice fringe pattern in this region [Fig. 7(c)] confirms that these layers correspond to CeO_2 imaged along a [110] projection. Moreover the alignment observed between the (111) diffraction spots of CeO_2 and those of Rh indicate that the decorating layers are epitaxially grown on the metal surface. This is entirely reasonable when we recall the epitaxial relationships described at the beginning of this section for Rh and Pt on ceria.

In Pt/CeO_2 and $Pt/CeTbO_x$ catalysts, similar decoration effects have been detected[16,17,38] after reduction in hydrogen at 973 K. Figure 7(d) shows precisely such an HREM image recorded on a 5% $Pt/Ce_{0.8}Tb_{0.2}O_2$ catalyst after reduction in pure hydrogen at 973 K for 1 h. Note that in this case the Pt particle is also surrounded at the bottom by a shell of support. On the uppermost (111) plane of this particle a row of black dots, with a separation of ~0.34 nm from each other, partially covering the surface, is also evident. This distance is much larger than that corresponding to the closest Pt atoms in the fcc structure, but matches fairly well with the distance of 0.33 nm between neighbouring lanthanide cations along the [1–12] direction of the $Ce_{0.8}Tb_{0.2}O_2$ oxide. This result indicates that these black dot contrasts observed at the surface cannot be assigned to the structure of the metal particle but should instead be ascribed to a coverage by a {111} support layer. Image calculations [Fig. 7(f)] further confirm this hypothesis. According to the structural model employed for this calculation [Fig. 7(e)], the black dot contrasts at 0.34 nm are due to a (111) $CeTbO_x$ cap covering the surface of the metal. This example allows us to address the question of how small or thin a decoration layer can be and yet still be detectable by HREM. According to the calculations presented here, even a submonolayer coverage could be detected in experimental images, like the one shown here, recorded in profile view conditions.

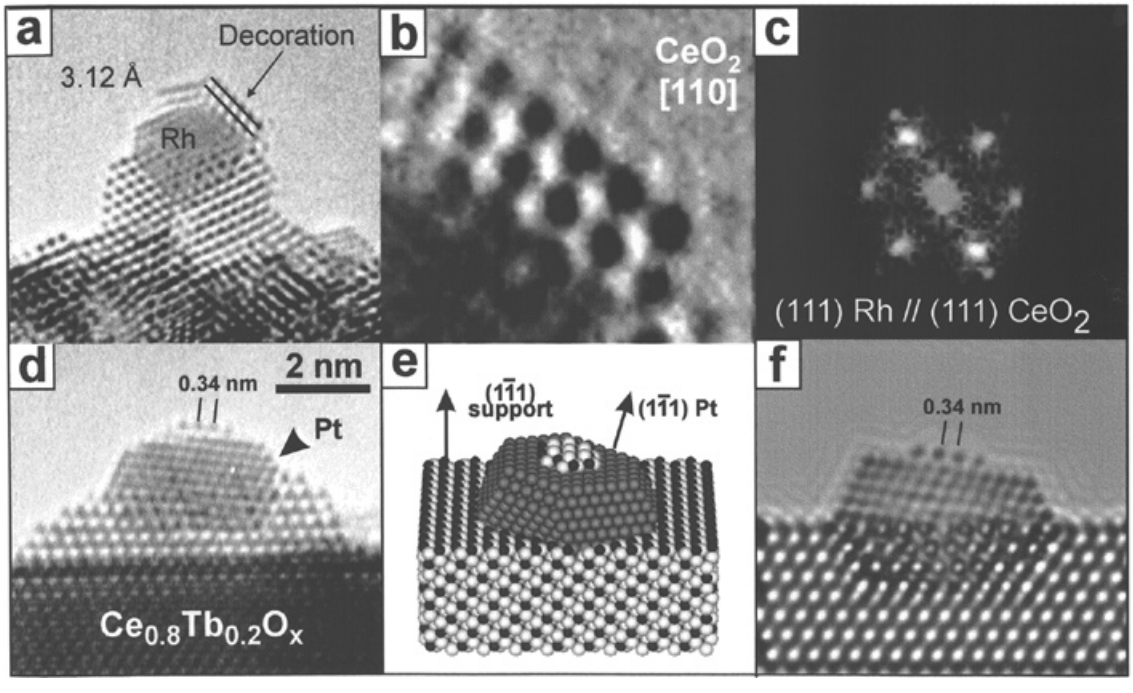

Figure 7. (a) Experimental image from a 2.5% Rh/CeO_2 catalyst reduced at 1173 K. (b) Detail of the surface of the experimental image. (c) The DDP obtained from the experimental image. (d) The HREM image from a 5% $Pt/Ce_{0.8}Tb_{0.2}O_2$ catalyst reduced at 973 K. (e) Supercell used as input for the calculation. (f) Simulated image.

CONCLUSIONS

From the set of examples analysed and discussed here an impression of the possibilities that HREM offers in the characterization of supported metal and oxide catalysts can be obtained. The use of image processing as a means to quantify the image contrast features, and of image simulation as a means to confirm structural hypotheses, is required to extract detailed information from the experimental images. In the case of supported metals, particle sizes of ~1 nm are large enough to carry out this detailed analysis, from which relevant conclusions about size, shape, chemical nature of the particles or their orientation relationships with the support can be drawn. Limitations of the technique in each particular case have been commented upon. In the field of supported oxides, the characterization of raft-like nanostructures has been shown to be feasible.

On assembling the different pieces of information related to the characterization of noble metals supported on ceria oxides, it seems clear that the structural features of metal–support interaction effects change continuously as a function of reduction temperature. Up to reduction temperatures of 973 K, Pt and Rh catalysts follow a parallel nanostructural evolution. Thus, in the reduction temperature range below 973 K the most remarkable aspect is the existence of metal–support orientation relationships in these catalysts. Increasing the temperature above 973 K leads to migration of the support on top of the metal particle surfaces, which as a result become partially covered. In the particular case of the Pt catalyst, further increases of the reduction temperature promote the alloying of metal atoms with the lanthanide atoms present in the support, resulting in the formation of hexagonal $LnPt_5$ intermetallic particles. Such an alloying process does not seem to take place in the case of Rh catalysts, where sintering and the formation of twins is the main effect of reduction treatments at the very high temperature regime.

The results obtained by HREM account for the contribution of structural aspects to the overall metal–support interaction effects. Additional contributions, which cannot be detected with this technique, can be operating in parallel or synergistically with the structural effects. This is the case of Pt supported on CeO_2 for example, where complementary chemical characterization data suggest that a contribution from electronic interactions with the support seems to be involved.

Acknowledgements

This work has received financial support from DGICYT (PB95-1257), CICYT (MAT96-0931) and MEC (Acciones Integradas España-Reino Unido. Ref: HB1997-0236). The experimental images were recorded at the EM Facilities of the SCCYT of the Universidad de Cádiz and at the Department of Materials Science and Engineering of the University of Liverpool.

REFERENCES

1. Ertl G, Knözinger H, Weitkamp J. *Handbook of Heterogeneous Catalysis*, vol. 1, Wiley-VCH: Weinheim, 1997.
2. Stevenson SA, Dumesic JA, Baker RTK, Ruckenstein E. *Metal–Support Interactions in Catalysis, Sintering, and Redispersion*. Van Nostrand Reinhold: New York, 1987.
3. Sánchez MG, Gázquez JL. *J. Catal.* 1987; **104**: 120.
4. Meriaudeau P, Dutel JF, Dufaux M, Naccache C. *Stud. Surf. Sci. Catal.* 1982; **11**: 95.
5. Meriaudeau P, Dufaux M, Naccache C. *Strong Metal/Support Interactions*, ACS Symposium Series vol. 298. American Chemical Society: Washington, 1986; 118.
6. Summers JC, Ausen SA. *J. Catal.* 1979; **58**: 131.
7. Tauster SJ, Fung SC, Garten RL. *J. Am. Chem. Soc.* 1978; **100**: 170.
8. Belzunegui JP, Sanz J, Rojo JM. *J. Am. Chem. Soc.* 1990; **112**: 4066.
9. Sanz J, Belzunegui JP, Rojo JM. *J. Am. Chem. Soc.* 1992; **114**: 6749.
10. Special issue: HRTEM for Catalysis. *Catal. Today* 1995: **23**(3).
11. Special issue: Electron Microscopy. *Catal. Rev. Sci. Eng.* 1992: **34**(1&2).
12. Special issue: Characterization of Catalysis. *Ultramicroscopy* 1990: **34**(1&2).
13. Bernal S, Botana FJ, Calvino JJ, López-Cartes C, Pérez-Omil JA, Rodríguez-Izquierdo JM. *Ultramicroscopy* 1998; **72**: 135.
14. Bernal S, Botana FJ, Calvino JJ, Cifredo GA, Pérez-Omil JA, Pintado JM. *Catal. Today* 1995; **23**: 219.
15. Bernal S, Botana FJ, Calvino JJ, López C, Pérez-Omil JA, Rodríguez-Izquierdo JM. *J. Chem. Soc. Faraday Trans* 1996; **92**: 2799.
16. Bernal S, Calvino JJ, Gatica JM, Larese C, López-Cartes C, Pérez-Omil JA. *J. Catal.* 1997; **169**: 510.
17. Bernal S, Calvino JJ, Cauqui MA, Gatica JM, Larese C, Pérez-Omil JA, Pintado JM. *Catal. Today* 1999; **50**: 175.
18. Burrows A, Kiely CJ, Pérez-Omil JA, Calvino JJ, Joyner RW. *Inst. Phys. Conf. Ser.* 1997; **153**: 395.
19. Burrows A, Kiely CJ, Perregaard J, Hojlund-Nielsen PE, Vorbeck G, Calvino JJ, López-Cartes C. *Catal. Lett.* 1999; **57**: 121.
20. Bernal S, Blanco G, Cauqui MA, Corchado MP, Larese C, Pintado JM, Rodríguez-Izquierdo JM. *Catal. Today* 1999; **53**: 607.
21. Pantazidis A, Burrows A, Kiely CJ, Mirodatos C. *J. Catal.* 1998; **177**: 325.
22. Stadelmann P. *Ultramicroscopy* 1987; **21**: 131.
23. Botana FJ, Calvino JJ, Blanco G, Marcos M, Pérez-Omil JA. *Electron Microsc.* 1994: **2B**: 1085.
24. Smith DJ, Glaisher W, Lu P, McCartney. *Ultramicroscopy* 1989; **29**: 123.
25. Reimer L. In *Transmission Electron Microscopy*, Springer Series in Optical Science vol. 36, MacAdam DL (ed). Springer Verlag: Berlin, 1984; 333–336.
26. Matyi RJ, Schwartz LH, Butt JB. *Catal. Rev.-Sci. Eng.* 1987; **29**: 41.
27. Bernal S, Calvino JJ, Cauqui MA, Pérez-Omil JA, Pintado JM, Rodríguez-Izquierdo JM. *Appl. Catal. B* 1998; **16**: 127.
28. Borodzinski A, Boranowska M. *Langmuir* 1997; **13**: 5613.
29. Harrison B, Diwell AF, Hallett C. *Platinum Metals Rev.* 1988; **32**: 73.
30. Yao MH, Smith DJ. *J. Microsc.* 1994; **175**: 252.
31. Klenov DO, Kryukova GN, Plyasova LM. *J. Mater. Chem.* 1998; **8**: 1665.
32. Radmilovic V, O'Keefe MA. *53rd Annu. Proc. MSA* 1995; 564.
33. Flüeli M. *Thesis*, Ecole Polytechnique Federale de Lausanne, Switzerland, 1989.
34. Rupprechter G, Seeber G, Hayek K, Hofmeister H. *Phys. Status Solids* 1994; **146**: 449.
35. Rupprechter G, Hayek K, Rendón L, José-Yacamán M. *Thin Solid Films* 1995; **260**: 148.

36. José-Yacamán M, Tehuacanero S, Zorrilla C. *Electron Microsc*. 1994; **2A**: 399.
37. Bernal S, Blanco G, Calvino JJ, Cifredo GA, Pérez-Omil JA, Pintado JM, Varo A. In *New Developments in Selective Oxidation II*, Cortés V, Vic S (eds). Elsevier Science: Amsterdam, 1994; 507–514.
38. Blanco G, Calvino JJ, Cauqui MA, Corchado P, López-Cartes C, Pérez-Omil JA, Colliex C, Stephan O. *Chem. Mater.* 1999; **11**: 3610.
39. Vainshtein BK. In *Modern Crystallography I*, Springer-Verlag Series in Solid State Sciences, Queisser HJ (ed). Springer Verlag: Berlin, 1981; 204–206.
40. Giorgio S, Henry C, Chapon C, Penisson JM. *J. Cryst. Growth* 1990; **100**: 254.
41. Smith DJ, Saxton WO, O'Keefe MA, Wood GJ, Stobbs WM. *Ultramicroscopy* 1983; **11**: 263.

